The Journal of Chemical Physics

How graphenic are graphynes? Evidence for low-lying correlated gapped states in graphynes

Cite as: J. Chem. Phys. **157**, 214704 (2022); https://doi.org/10.1063/5.0125637
Submitted: 13 September 2022 • Accepted: 11 November 2022 • Accepted Manuscript Online: 14 November 2022 • Published Online: 07 December 2022

Genís Lleopart, Miquel Lopez-Suarez, Ibério de P. R. Moreira, et al.

The Journal of Chemical Physics ARTICLE scitation.org/journal/jcp

How graphenic are graphynes? Evidence for low-lying correlated gapped states in graphynes

Cite as: J. Chem. Phys. 157, 214704 (2022); doi: 10.1063/5.0125637
Submitted: 13 September 2022 • Accepted: 11 November 2022 •
Published Online: 7 December 2022

Genís Lleopart,[1] Miquel Lopez-Suarez,[1] Ibério de P. R. Moreira,[1,a)] and Stefan T. Bromley[1,2,a)]

AFFILIATIONS

[1] Departament de Ciència de Materials i Química Física and Institut de Química Teòrica i Computacional (IQTC), Universitat de Barcelona, c/ Martí i Franquès 1-11, 08028 Barcelona, Spain

[2] Institució Catalana de Recerca i Estudis Avançats (ICREA), Passeig de Lluís Companys, 23, 08010 Barcelona, Spain

[a)] **Authors to whom correspondence should be addressed:** i.moreira@ub.edu and s.bromley@ub.edu

ABSTRACT

Graphynes can be structurally envisioned as 2D extensions to graphene, whereby linearly bonded carbon linkages increase the distance between trigonal carbon nodes. Many graphynes have been predicted to exhibit a Dirac-like semimetallic (SEM) graphenic electronic structure, which could potentially make them competitive with graphene for applications. Currently, most graphynes remain as attractive synthetic targets, and their properties are still unconfirmed. Here, we demonstrate that the electronic structure of hexagonal α-graphyne is analogous to that of biaxially strained graphene. By comparison with accurate quantum Monte Carlo results on strained graphene, we show that the relative energetic stability of electronic states in this correlated 2D system can be captured by density functional theory (DFT) calculations using carefully tailored hybrid functionals. Our tuned hybrid DFT approach confirms that α-graphyne has a low energy correlated Mott-like antiferromagnetic insulating (AFI) state, which competes with the SEM state. Our work shows that the AFI-SEM crossover in α-graphyne could be tunable by in-plane biaxial strain. Applying our approach to other graphynes shows that they should also exhibit correlated AFI states, which could be dominant even at zero strain. Calculations using an onsite Coulombic repulsive term (i.e., DFT + U) also confirm the predictions of our hybrid DFT calculations. Overall, our work strongly suggests that graphynes are not as graphenic (i.e., Dirac-like) as often previously predicted by DFT calculations using standard generalized gradient approximation functionals. However, due to the greater electronic versatility (e.g., tunable semiconducting bandgaps and accessible spin polarized states) implied by our study, graphynes could have novel device applications that are complementary to those of graphene.

INTRODUCTION

Structurally, graphynes can be regarded as 2D extensions of graphene in which linearly linked sp-hybridized carbon centers have been periodically inserted between selected neighboring sp^2 carbon centers of the graphenic sheet.[1] Although most graphynes are yet to be experimentally realized, they have been widely proposed as a promising new class of versatile 2D materials for a range of applications.[2–5] In particular, numerous graphynes have been predicted to possess band structures with Dirac cones near the Fermi level, potentially allowing for a new range of electronically versatile and high-mobility graphene-like materials.[6–8] Symmetrically expanding graphene's hexagonal lattice with a linear acetylenic (–C≡C–) bridge between all carbon atoms gives rise to α-graphyne. The distance between carbon centers in graphene can also be symmetrically extended by in-plane biaxial strain. In both biaxially strained graphene and chemically extended α-graphyne, the interaction between trigonal sp^2 carbon nodes in graphene is diminished, thus decreasing the tendency for electronic delocalization. For graphene, many-body quantum Monte Carlo (QMC) calculations have shown that in-plane biaxial strain destabilizes its high mobility semimetallic (SEM) character while inducing the appearance of gapped solutions [e.g., correlated Mott-like antiferromagnetic insulator (AFI) and topological dimerized states].[9,10] Using these results as a reference, we use carefully tuned hybrid density functional theory (DFT) calculations to assess to what extent chemically expanded graphenes (i.e., graphynes) mimic the behavior of mechanically expanded graphene. Our study provides evidence that the gapless

Dirac-like SEM character of α-graphyne is highly susceptible to electron localization and the emergence of a correlated gapped AFI state. Specifically, our results imply that the electronic structure of unstrained α-graphyne lies close to a SEM-AFI crossover and could be tuned to exhibit either state through modest in-plane strain. Furthermore, we use this tuned DFT approach to more generally confirm that correlated gapped AFI states can be more energetically stable than graphenic SEM states for other graphynes, even when unstrained. These results are also corroborated by DFT + U calculations. Overall, our findings strongly suggest that gapped correlated AFI states in graphynes should be significantly easier to access than in graphene. Correspondingly, our results imply that graphynes could be very attractive systems for both device technologies and fundamental studies of low dimensional correlated materials.

METHODOLOGY

For all DFT calculations employing hybrid functionals, we used the Fritz Haber Institute *ab initio* materials simulation (FHI-AIMS) package,[11] which employs all-electron atom-centered numerical basis functions for ensuring highly accurate results.[12] Specifically, we employed hybrid functionals based on the generalized gradient approximation (GGA) Perdew–Burke–Ernzerhof (PBE)[14] functional, which incorporated variable proportions of exact Hartree–Fock exchange (HFE). We refer to this set of functionals as PBE-X, where X is the percentage of HFE used. For all these calculations, we employed a Tier 1 light basis set that provides results of similar or higher quality to those obtained using a triple-zeta plus polarization atomic Gaussian type orbital basis set.[14] For our comparisons with the results in Ref. 10, we employ a 3 × 3 × 1 supercell of graphene containing 24 carbon atoms and a 12 × 12 × 1 Monkhorst–Pack (MP) **k**-point sampling grid of reciprocal space vectors. For α-graphyne, β-graphyne, 6-6-12-graphyne, δ-graphyne, and p-graphyne, single unit cell calculations were employed with suitably converged **k**-point sampling grids using the MP scheme. Unstrained systems were fully optimized until forces on each atom were less than 0.01 eV/Å. For graphene and α-graphyne, the lattice parameters were uniformly varied to induce biaxial strains between −5% and 26%, and in each case, they were kept fixed while all internal structural degrees of freedom of the system were relaxed. We repeated these strain calculations for all relevant electronic solutions.

Estimates of effective U and t values were derived from the above DFT-calculated all-electron band structures and used to physically characterize the electronic state of our systems. Following our previous work,[15] we extract approximate U and t values based on considering a generalized Heisenberg model description of a fully localized AFI system.[16] Here, $U = E_g$, where E_g is the bandgap and t can be derived from $W = \frac{2zt^2}{U}$, where W is the width of the valence band and z is the number of nearest neighbors (three for a 2D hexagonal lattice). Note that, by definition, U (and thus U/t) is zero for gapless semimetallic states, and reported finite values characterize AFI states. For the extraction of U and t values for graphene, we used the primitive two atom cell with a relatively denser 24 × 24 × 1 k-grid. Although the absolute values of extracted effective U and t values from DFT calculations cannot be directly compared with those used in many-body Hamiltonian models, the electronic character of the system with respect to varying U/t should be analogous.

We also performed DFT + U calculations using the pure GGA-based PBE functional in which an effective on-site Coulomb interaction (U_{eff}) was added to treat $2p_z$ electrons on all carbon centers. We employed the simplified rotationally invariant DFT + U formulation of Dudarev *et al.*[17] as implemented in the Siesta package,[18] where $U_{\text{eff}} = U - J$, and U and J are the intra-atomic Hubbard on-site Coulombic interaction and the exchange integral, respectively. For Hubbard projectors, slightly-excited numerical atomic orbitals were employed with a radius set to 0.95 Å. We used a double-ζ polarized basis set to expand the one-electron wave-function, while core electrons were accounted for by means of norm-conserving pseudopotentials. A converged MP grid of k-points to sample the Brillouin zone was used for each system, and structures were relaxed until the atomic forces were less than 0.01 eV/Å.

RESULTS AND DISCUSSION

Comparing DFT and QMC results for biaxially strained graphene

Graphene is an example of a half-filled 2D hexagonal lattice (i.e., one "free" electron per carbon lattice node) in which the competing tendencies of electron delocalization/localization can be approximately described by the Hubbard model.[19] This approximate model uses a Hamiltonian with two parameters to capture: (i) the Coulombic repulsion between single electrons on the same lattice site (U) and (ii) the hopping integral between nearest neighbor sites (t). Solving the Hubbard model Hamiltonian on the rigid 2D hexagonal lattice yields a phase diagram exhibiting a delocalized SEM solution when $U/t \lesssim 3.9$ and a continuous phase transition to a Mott-like AFI solution for $U/t \gtrsim 3.9$.[20] Using an accurate off-lattice QMC approach, the Hubbard model has also been solved for biaxially strained graphene.[10] These calculations reveal that with increasing in-plane strain, dimerized insulating states appear before, and always dominate, the AFI solution. Unlike spin-polarized AFI states, dimerized states are closed-shell in nature, where the sp_z electrons participate in local π bonds.

Standard DFT methods based on the GGA calculations on biaxially strained graphene predict the emergence of dimerized solutions at relatively high in-plane strains but do not capture the AFI solution.[21] The GGA approximation to DFT is well known to poorly describe correlated materials; however, calculations using hybrid functionals that incorporate a fraction of HFE can largely correct this deficiency. The resulting hybrid DFT-based methods have become very effective approaches to investigate the electronic structure of different types of materials, ranging from strongly correlated transition metal oxides (e.g., cuprates,[22] NiO,[23,24] and manganites[25]) to organic radicals[26] and polyradicals,[27–29] with a remarkable reliability in describing their ground states and magnetic properties. In such studies, although the quantitative results are sensitive to the exact percentage of HFE employed, most hybrid functionals use between 20% and 50% HFE and provide qualitatively similar results. In our previous work on 2D covalent organic frameworks (COFs) based on hexagonal networks sp^2 carbon centers, we found that hybrid functionals could describe both their low energy multiradical (AFI) and quinoidal (dimerized) states.[30,31] By careful comparison with available experimental data, we found that the PBE0[15] hybrid functional (25% HFE) was a good choice for accurately describing

these correlated Mott insulating systems.[32] Calculations using the Heyd–Scuseria–Ernzerhof (HSE) functional[33] (a short-range screened version of PBE0) to describe biaxially strained graphene,[10,34] capture both the AFI and dimerized solutions (unlike GGA). However, HSE calculations invert the stabilities of the AFI and dimerized solution with respect to QMC calculations. Unlike the highly correlated localized electrons in 2D sp^2-based hexagonal COFs, the localization of electrons in the AFI state of strained graphene emerges from a low energy weakly correlated SEM state. This suggests that functionals with a lower tendency for electron localization than HSE may be more suitable to describe the electronic structure of strained graphene.

In Fig. 1(a), we show the predicted relative energetic stability of the three considered electronic solutions of graphene with respect to biaxial strain (ε) using the hybrid PBE0 functional as compared with the corresponding QMC results from Ref. 10. Both sets of QMC results predict an initial stabilization of the dimerized state at approximately ε = 8% and a subsequent stabilization of the AFI state for ε = 12%–15%. Our PBE0 results confirm reported DFT results using the HSE functional,[10] where, unlike in the QMC calculations, the AFI solution becomes more stable than the SEM solution (at ε ≈ 7%) before the dimerized solution starts to stabilize (ε ≈ 10%) with increasing strain. With further increases in biaxial strain, PBE0 and HSE based DFT calculations predict a subsequent crossover in energetic stability between the dimerized and AFI solutions, which is not observed in the QMC calculations. In Fig. 1(a), we also include

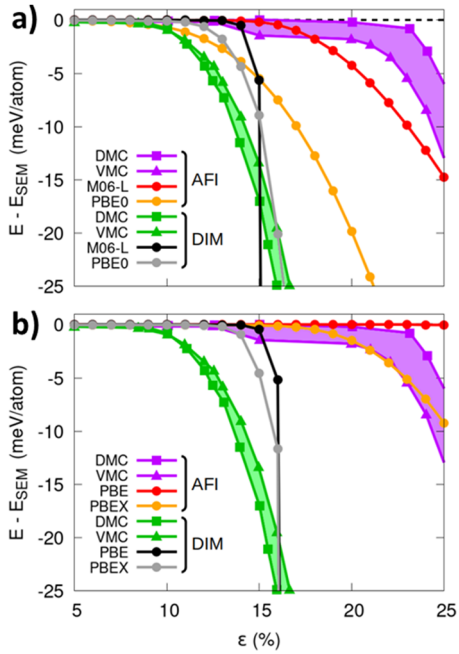

FIG. 1. Comparison of the energies of the AFI and dimerized (DIM) electronic solutions with respect to the SEM solution in graphene with respect to biaxial strain (ε) using the QMC results from Ref. 10 (from both VMC and DMC calculations) as a reference. In (a), we compare the QMC data with results from DFT calculations using the hybrid PBE0 functional and the meta-GGA M06-L functional, and in (b), we compare the QMC data with results from DFT calculations using the pure-GGA PBE functional and a tuned hybrid PBE-X functional with X = 12.5%.

results from DFT calculations using the M06-L[35] meta-GGA functional. Meta-GGA functionals are parameterized by also considering the second derivative of the electron density, in addition to just the first derivative in standard GGA functionals, and the kinetic energy density. The M06-L calculations predict the correct order of the stabilization of the dimerized and AFI solutions with respect to the QMC results. However, the onset of the dimerized solution occurs at an even higher strain (ε ≈ 13%) than in the PBE0 calculations, with the subsequent stabilization of the AFI solution starting very quickly afterward (ε ≈ 15%). Although the latter AFI onset strain is in line with the QMC results, the subsequent strain-dependent behavior of the AFI solution with respect the SEM solution described by M06-L tends to be over-stabilizing.

In Fig. 1(b), we show the results obtained from reducing the proportion of HFE in the PBE0 functional by one-half to 12.5% (i.e., PBE-12.5). Here, as for the M06-L results, we see that the AFI solution becomes more stable than the SEM solution at a higher strain than that at which the dimerized solution becomes energetically dominant. However, the PBE-12.5 calculations show an improvement over the M06-L results with respect to the relatively lower onset strain of the dimerized solution and the strain dependent energetics of the AFI solution, both of which are more in line with the QMC results. We note that a similar improvement in the agreement between hybrid DFT and QMC can be achieved by using 12.5% HFE in the screened HSE functional (see the supplementary material). In Fig. 1(b), we also include the results from pure GGA PBE calculations. Here, the onset of the dimerized solution at a relatively high biaxial strain (ε ≈ 14%) and the AFI solution cannot be energetically stabilized relative to the SEM state (i.e., the system always falls into the SEM solution).

Generally, all tested DFT functionals can stabilize the dimerized solution within a fairly consistent range of biaxial strains (11% ≤ ε ≤ 14%), albeit at a somewhat higher strain than predicted by QMC calculations. This delayed onset of the dimerized solution in a DFT treatment may indicate a mixing between dimerized and SEM solutions, tending to stabilize the former. The description of the onset strain and strain-dependent energetic stability of the AFI solution is found to be much more sensitive to the functional employed. Overall, the comparative plots in Fig. 1 show that hybrid DFT calculations with a suitable percentage of HFE can provide an electronic description of biaxially strained graphene that is consistent with that from accurate calculations using many-body effective Hamiltonians. We stress that the relative energetics of the strain dependent SEM to AFI transition described by our PBE-12.5 calculations is in near quantitative agreement with the two QMC approaches. In the following section, we will focus on the competition between SEM and AFI solutions in both biaxially strained graphene and α-graphyne using DFT calculations.

Comparing the electronic structure of biaxially strained graphene and α-graphyene

In addition to relative energetic stability, the SEM and AFI solutions can be differentiated by their physical characteristics. For example, unlike the delocalized SEM solution, the AFI solution corresponds to a lattice of localized unpaired electrons with a net absolute spin moment per sp^2 carbon center. This correlated spin-localized state is stabilized by relatively high U/t ratios. In the

Hubbard model, U and t are freely variable parameters that attempt to capture the influence of the full quantum system on an accurately described subset of electrons. DFT calculations provide a more approximate quantum mechanical description but treat all electrons in the system. In Figs. 2(b)–2(d), we show how the SEM and AFI solutions in graphene vary with respect to biaxial strain and the degree of HFE in the PBE-X functional employed for (b) relative energy with respect to the SEM solution ($E - E_{SEM}$), (c) average absolute spin moment per trigonal carbon site ($|\langle\mu_{3C}\rangle|$), and (d) the U/t ratio.

In Fig. 2(b), the strain-dependent relative energy difference is low and constant for lower strains when in the SEM solution before reaching a strain at which it rapidly increases with further strain increase, indicating a transition to the AFI solution. The change in $E - E_{SEM}$ during the SEM-to-AFI crossover is continuous (pointing to mixing of the AFI solution with the SEM solution), and the turning points in each curve occurring at ~0.2 meV/atom indicate the crossover strain magnitude. The SEM-to-AFI crossover is more clearly confirmed in the more stepwise behavior of $|\langle\mu_{3C}\rangle|$ [Fig. 2(c)] and U/t [Fig. 2(d)]. Both these descriptors are zero in the SEM state and abruptly show a finite value for any sign of the AFI solution. The SEM-AFI crossover values of $|\langle\mu_{3C}\rangle|$ and U/t are found to be ~0.025 and 0.5, respectively. This suggests that conjugation effects are significant in stabilizing the system. The overall character of the SEM-AFI crossover is not significantly changed by varying X in the PBE-X calculations, but higher X values push the system toward the AFI state for smaller strains, while lower X values help preserve the SEM state with respect to the strain increase. Our tuned X value of 12.5 leads to a SEM-AFI crossover at 12%–13% biaxial strain. Note that for pure PBE, the AFI solution only emerges at unphysically large applied strains (i.e., close to atomic dissociation).

Following the same hybrid DFT based methodology, we studied how the SEM and AFI solutions for α-graphyne depend on biaxial strain. We note that in the case of α-graphyne, localization of all electrons in a bonded solution (analogous to a dimerized state in graphene) would entail that a proportion of the acetylenic linkages become cumulenic (i.e., C=C=C=C). The acetylenic linkages between sp^2 centers in graphynes are predicted to exhibit very little resonance with the cumulenic form.[1] Even in our PBE calculations for the most delocalized SEM solution of α-graphyne, the acetylenic linkers were characterized by typical 1.39 Å C–C single bonds and 1.23 Å C≡C triple bonds. We were unable to stabilize any solution with uniform cumulenic linkages for any strain. This can be understood as elongation induced by biaxial strain further stabilizes localization of triple bonds [compare, for instance, 2-butyne (1.47 Å C–C and 1.21 Å C≡C leading to 4.15 Å between terminal C) with 1,2,3-butatriene ($C^{\alpha}=C^{\beta}=C^{\beta}=C^{\alpha}$ with 1.32 Å $C^{\alpha}=C^{\beta}$ and 1.28 Å $C^{\beta}=C^{\beta}$ leading to 3.92 Å between terminal C)].[36] Experimental studies on simple C_{18} ring structures also show a stabilizing preference for acetylenic linkages over cumulenic forms.[37] With respect to this study, it is interesting to note that the experimental structure of C_{18} can only be accurately described by DFT when using hybrid functionals with a significant proportion of HFE.[38] As such, AFI solutions are expected to be the lowest energy non-SEM electronic states in α-graphyne. In Fig. 3, we show how the SEM and AFI solutions vary in α-graphyne with respect to biaxial strain, value of X employed, as well as $|\langle\mu_{3C}\rangle|$ and the U/t ratio.

As in the case of biaxially strained graphene, all three descriptors tend to be more constant in the SEM solution and then crossover to a rapidly increasing regime in the AFI solution. We note that in α-graphyne, in addition to spin polarization on sp^2 centers, we also find patterns of AFI-like alternating spin polarization

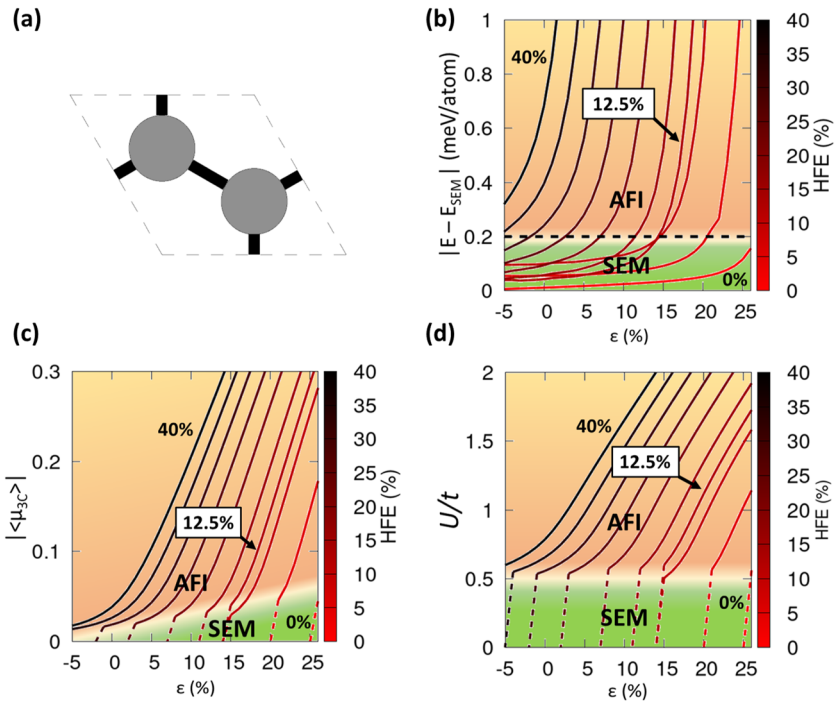

FIG. 2. Effect of biaxial strain on the properties of graphene using the unit cell shown in (a). The plots show how the SEM (green) and AFI (light brown) solutions are affected by strains between −5% and 26% as described by DFT calculations using PBE-X functionals with X = 0%–40% with respect to (b) energy relative to the SEM solution ($|E - E_{SEM}|$), (c) average absolute spin moment per trigonal carbon (3C) site ($|\langle\mu_{3C}\rangle|$), and (d) U/t. In all cases, the curves derived from using the tuned PBE-12.5 functional [see Fig. 1(b)] are labeled. The lighter shaded area in each plot denotes the approximate SEM-AFI crossover regime.

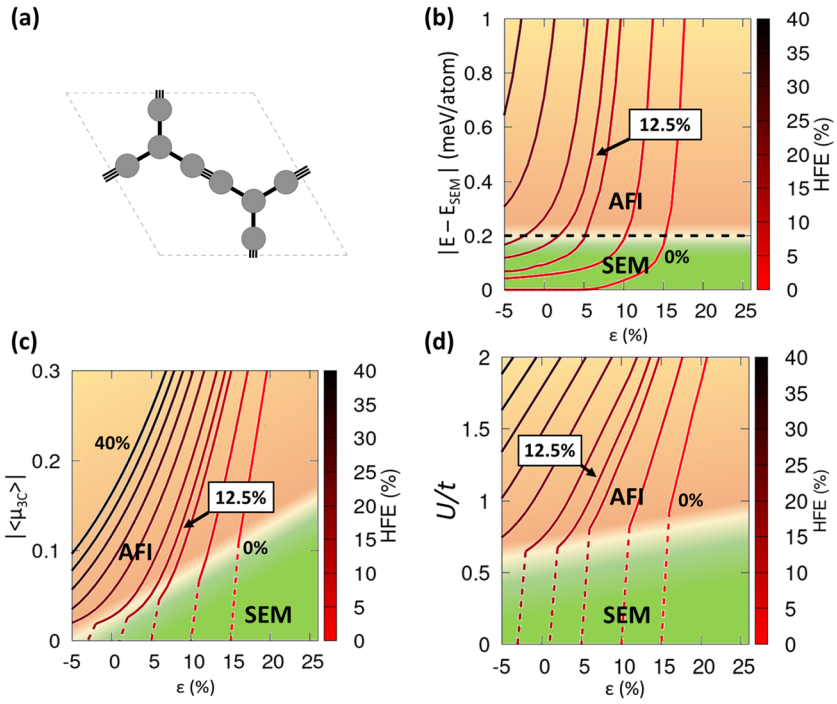

FIG. 3. Effect biaxial strain on the properties of α-graphyne—unit cell shown in (a). The plots show how the SEM (green) and AFI (light brown) solutions are affected by strains between −5% and 26% as described by DFT calculations using PBE-X functionals with X = 0%–40% with respect to (b) $E - E_{SEM}$, (c) $|\langle\mu_{3C}\rangle|$, and (d) U/t. In all cases, the curves derived from using the tuned PBE-12.5 functional used in Fig. 1(b) are labeled. The lighter shaded area in each plot denotes the approximate SEM-AFI crossover regime.

on the acetylenic linkers between sp^2 centers. We also note that, in the region of change of each of the descriptors (i.e., the SEM-AFI crossover), the value ranges of $|E - E_{SEM}|$, $|\langle\mu_{3C}\rangle|$, and U/t are all largely consistent with the SEM-AFI crossover values for strained graphene. Although having a similar general dependence on strain, the strain at which the crossover occurs in α-graphyne for any value of X is shifted to a lower strain with respect to the corresponding crossover in graphene. As α-graphyne has an expanded graphene-like hexagonally symmetric structure, this strongly suggests that α-graphyne behaves like a "pre-strained" graphene with respect to the SEM-AFI transition. To test this proposal, we assume that the electronic structure of α-graphyne can be approximately captured by that of 13% biaxially strained graphene. By setting a common zero strain for both systems, we see that the PBE-12.5 calculated values of both $|\langle\mu_{3C}\rangle|$ and U/t follow an extremely similar dependence on strain during the SEM-AFI crossover (see Fig. 4).

The above comparative analysis strongly confirms the close correspondence between the electronic structure of biaxially strained graphene and α-graphyne. Following the excellent agreement of our PBE-X DFT calculations (using X = 12.5) with QMC results for the SEM-AFI crossover in strained graphene [see Fig. 1(b)], we propose that PBE-12.5 should be similarly suitable for accurately describing the SEM-AFI crossover in α-graphyne. Most previously reported DFT calculations have used non-hybrid generalized gradient approximation (GGA) functionals to predict that unstrained α-graphyne is a Dirac material with a stable SEM solution.[5–7] Calculations employing the screened hybrid HSE functional (X = 25) have conversely found that the AFI solution is dominant in α-graphyne for low strains.[39] From Fig. 3, we confirm that for X > 20, the AFI solution is more stable than the SEM solution even for zero strain. Likewise, for approximately X < 12.5, the SEM solution tends to be more favored for zero to moderate strain. However, when using the tuned value of X = 12.5, we see that unstrained α-graphyne is predicted to be electronically very close to the crossover regime between SEM and AFI solutions. In Fig. 5(a), we see that the PBE-12.5-calculated band structure of unstrained α-graphyne is found to have a correspondingly small gap (~0.2 eV). We note that small perturbations to the structure of α-graphyne (e.g., thermal excitation and induced epitaxial strain upon adsorption on a surface) would likely further open its gap. The closeness to both a high mobility SEM state and a AFI correlated gapped state points to α-graphyne being a highly attractive material for both device applications and as a flexible 2D system for studying correlated electronic transitions.

Correlated gapped AFI states in other graphynes

Based on the above results, we more generally propose that DFT calculations using functionals with a moderate amount of HFE (~12.5%) are likely to be appropriate for describing the competition between SEM and AFI states in other 2D systems of sp-linked sp^2 carbon centers. We also note that for moderately strained graphene, where all sp^2 carbon centers are directly linked, our PBE-12.5 approach correctly recovers the stable SEM solution. As such, our tuned DFT approach is also likely to be suitable for describing other 2D graphynes with mixtures of direct and acetylenic linkages between sp^2 carbon centers in which correlated AFI states

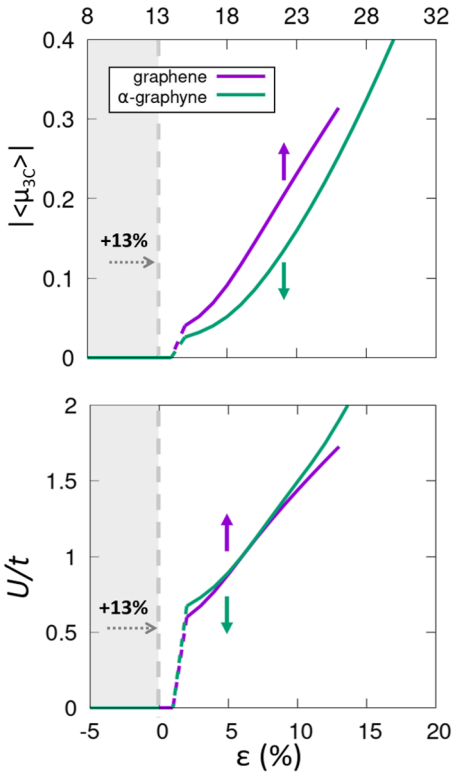

FIG. 4. Comparison of $|\langle\mu_{3C}\rangle|$ (upper) and U/t (lower) for 13% biaxially strained graphene (purple lines; upper axis) and unstrained α-graphyne (green lines; lower axis) with respect to biaxial strain.

and Dirac-like SEM states could compete. Directly linked sp^2 centers also imply the possibility of alternative electronic solutions where electron sharing could lead to local double bonds between such sites. For all the systems described below, we were unable to stabilize solutions with local double bonds between neighboring sp^2 centers. We note that all bond distances vary by less than 0.025 Å for all calculations for each respective unstrained structure reported below. Even with the application of strain, we argue that such simple "dimerized" states are unlikely to be stabilized as the resulting local C=C bonds are much less stable than more extended units that showing increased resonance that stabilizes the system.[40,41] Hence, it is expected that strain would induce more stable perethynylated fragments such as tetraethylethene, hexaethynylbenzene, or diethynylallene analogs,[41] instead of smaller ethylenic, acetylenic, or benzenic fragments, leading to a complex fragmentation (and reorganization) of the system beyond its elastic limit.

In Figs. 5(b)–5(e), we show the geometric structures of four graphynic systems with mixtures of direct and single acetylenic linkages between sp^2 carbon centers: β-graphyne, δ-graphyne, and 6-6-12 graphyne (first reported in Ref. 1) and a structure also exhibiting double-acetylenic linkages parallelogrammatic graphyne[42] (referred to hereafter as p-graphyne). For each structure, we report the electronic band structure as calculated using PBE, PBE-12.5, and PBE0. As for α-graphyne, DFT calculations using the pure GGA PBE functional predict that all these 2D systems have dominant SEM-like solutions with Dirac cone band crossings near to the Fermi level (see gray PBE band structures in Fig. 5). The details of these Dirac-like electronic band structures have been discussed in detail in previous studies.[5–7,42] The incorporation of 12.5% HFE is found to open a gap for all the GGA-predicted Dirac cone band crossings. Furthermore, unlike α-graphyne, this occurs for all materials without any in-plane strain. For β-graphyne, a single gap of 0.84 eV is observed, whereas two gaps of 0.36 and 0.62 eV are found for 6-6-12 graphyne. For δ-graphyne and p-graphyne, only relatively small gaps of 0.1 and 0.17 eV, respectively, are opened up.

To verify that these bandgap openings correspond to a correlated AFI state in each case, we extract $|\langle\mu_{3C}\rangle|$ and U/t in each case. For β-graphyne and 6-6-12 graphyne, we find $|\langle\mu_{3C}\rangle|$ values of 0.1, and 0.05, respectively, which are both larger than the SEM-AFI crossover value of ~0.025 found for strained graphene and α-graphyne (see Figs. 2 and 3). For δ-graphyne and p-graphyne, the relatively low values of $|\langle\mu_{3C}\rangle|$ of 0.010 and 0.004 (rounded to zero in Fig. 5) indicate that they are also close to a SEM-AFI crossover, in line with their small bandgaps. For U/t ratios, we find values of 1.83 and 1.02 for β-graphyne and 6-6-12, respectively, which are again both above the SEM-AFI crossover value of ~0.6 found for strained graphene and α-graphyne (see Figs. 2 and 3). These results suggest that β-graphyne and 6-6-12 graphyne would be even more susceptible to exhibit an AFI state than α-graphyne. For δ-graphyne and p-graphyne, the very similar U/t values of 0.64 and 0.63, respectively, are very similar to that corresponding to the SEM-AFI crossover for strained graphene and α-graphyne. This suggests that δ-graphyne and p-graphyne, like α-graphyne, may be other attractive 2D platforms for exploring highly tunable correlated electronic states. We note that our approach is tuned for 2D carbon-based sp^2-linked systems in which there is a competition between a SEM solution and a correlated gapped AFI solution. As such, our approach is not tailored for accurately describing sp^2-based systems where semiconducting gaps arise due to the specific details of the electronic band structure (e.g., γ-graphyne[5]) and are not induced by electron correlation.

To further confirm that the stable AFI solutions revealed by our hybrid PBE-X calculations are primarily due to a U/t-based localization of unpaired electrons (i.e., a correlated Mott insulator type transition), we examine a simplified description of our four considered graphynes using DFT + U calculations. In our DFT + U calculations, an effective onsite U_{eff} parameter is chosen and then applied to $2p_z$ electrons on each carbon atom within spatially localized regions by means of atomic orbital projectors. We note that this is unlike hybrid DFT calculations in which the chosen percentage of HFE consistently affects all electrons, and then, U and t are extracted. In particular, the value of U extracted from the latter cannot be quantitatively compared with U_{eff}, where it is used to define the energy functional in a DFT + U calculation, although their qualitative effect on electronic structure should be similar. Choice of an appropriate U_{eff} values for a particular element/orbital can depend significantly on the details of the particular DFT + U implementation used to include this local correction in the description of the electronic band structure of the system.[43] For the PBE functional and the simplified, rotationally invariant formulation of DFT + U,[17] as both used in this work, self-consistent *ab initio* U_{eff} parameters for

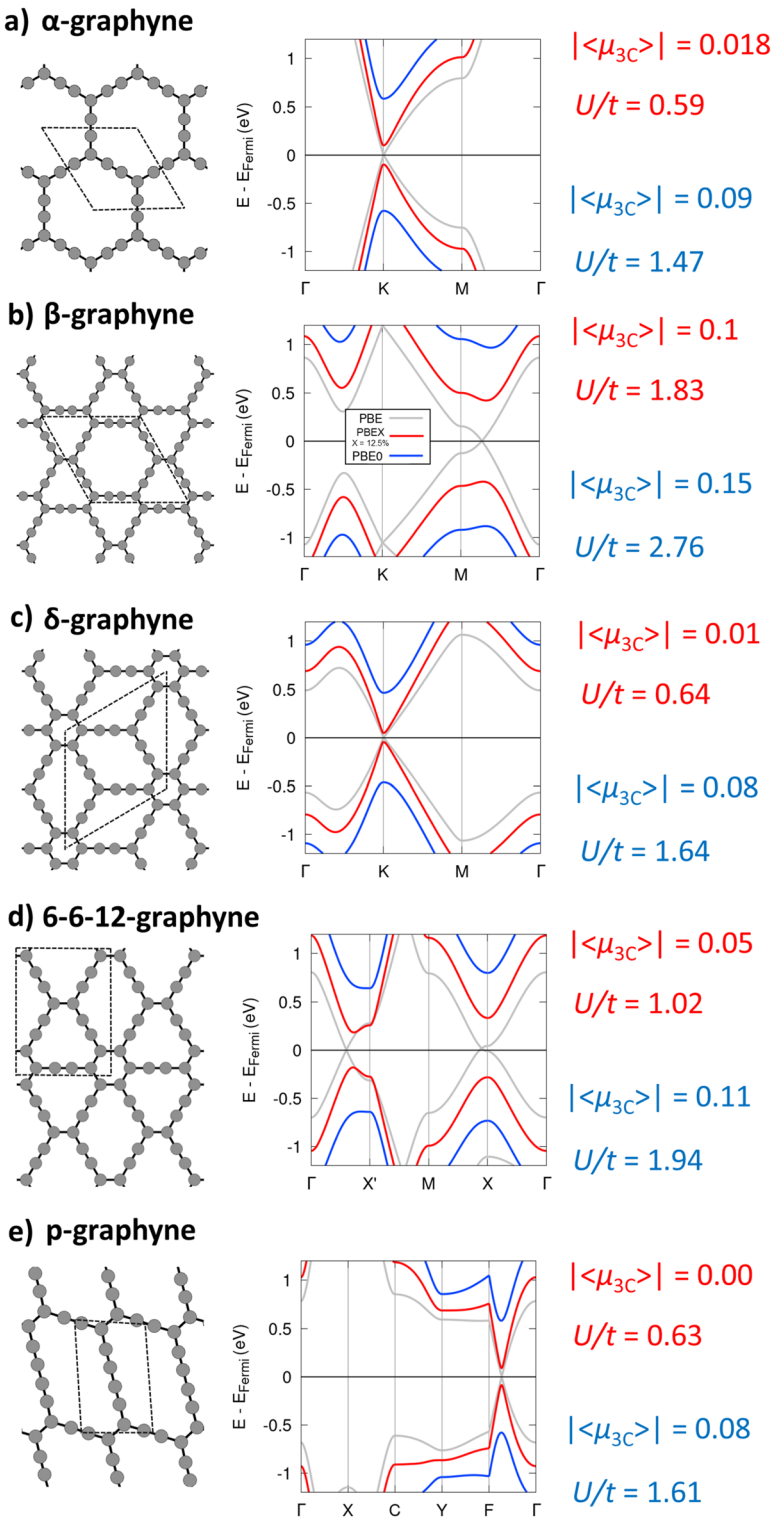

FIG. 5. Electronic band structures of (a) α-graphyne, (b) β-graphyne, (c) δ-graphyne, (d) 6-6-12 graphyne, and (e) p-graphyne (see structures left). The regions delimited by dashed lines show the unit cell used in the respective calculations. Corresponding electronic band structures are shown to the right. The gray bands are obtained with DFT calculations using the pure GGA (PBE) functional. The red bands are obtained using the tuned PBE-12.5 hybrid functional, and the blue bands correspond to PBE0 calculations.

PBE + U calculations have been obtained from density-functional perturbation theory.[44] Here, the lowest U_{eff} values obtained for 2p orbitals of light elements (N and O) are around 6.5–7 eV. As a similar magnitude is expected for the $2p_z$ orbitals of carbon, we ran two sets of PBE + U calculations with U_{eff} values of 5 and 7.5 eV, respectively. In Fig. 6, we show the PBE + U band structures for α-graphyne, β-graphyne, δ-graphyne, 6-6-12 graphyne, and p-graphyne. We see that for U_{eff} = 5 eV unstrained β-graphyne, δ-graphyne, and 6-6-12 graphyne all exhibit significant bandgaps (>0.25 eV), albeit slightly smaller than found for the corresponding PBE-12.5 calculations. For this relatively small U_{eff} value, both α-graphyne and p-graphyne exhibit a non-gapped SEM solution, whereas they are found to have a very small gap in the respective PBE-12.5 calculations. For a slightly larger U_{eff} value of 7.5 eV, all systems show a significant gap opening. β-graphyne, δ-graphyne, and 6-6-12 graphyne all display gaps of >0.8 eV, and α-graphyne and p-graphyne now display >0.3 eV gaps.

In general, both PBE-X and PBE + U sets of results are qualitatively consistent, which confirms that the electronic structure of these materials is determined by the degree of electron localization of unpaired electrons in the AFI state. Our results imply that unstrained β-graphyne and 6-6-12 graphyne are intrinsically gapped AFI materials and are thus the least graphenic graphynes of those considered. More interestingly, we predict that unstrained α-graphyne, δ-graphyne, and p-graphyne are likely to have graphene-like Dirac-like SEM ground states but, unlike graphene, are easily perturbed (e.g., via moderate biaxial strain) into correlated AFI states. Much like twist-tunable bilayer graphene,[45] single-layer

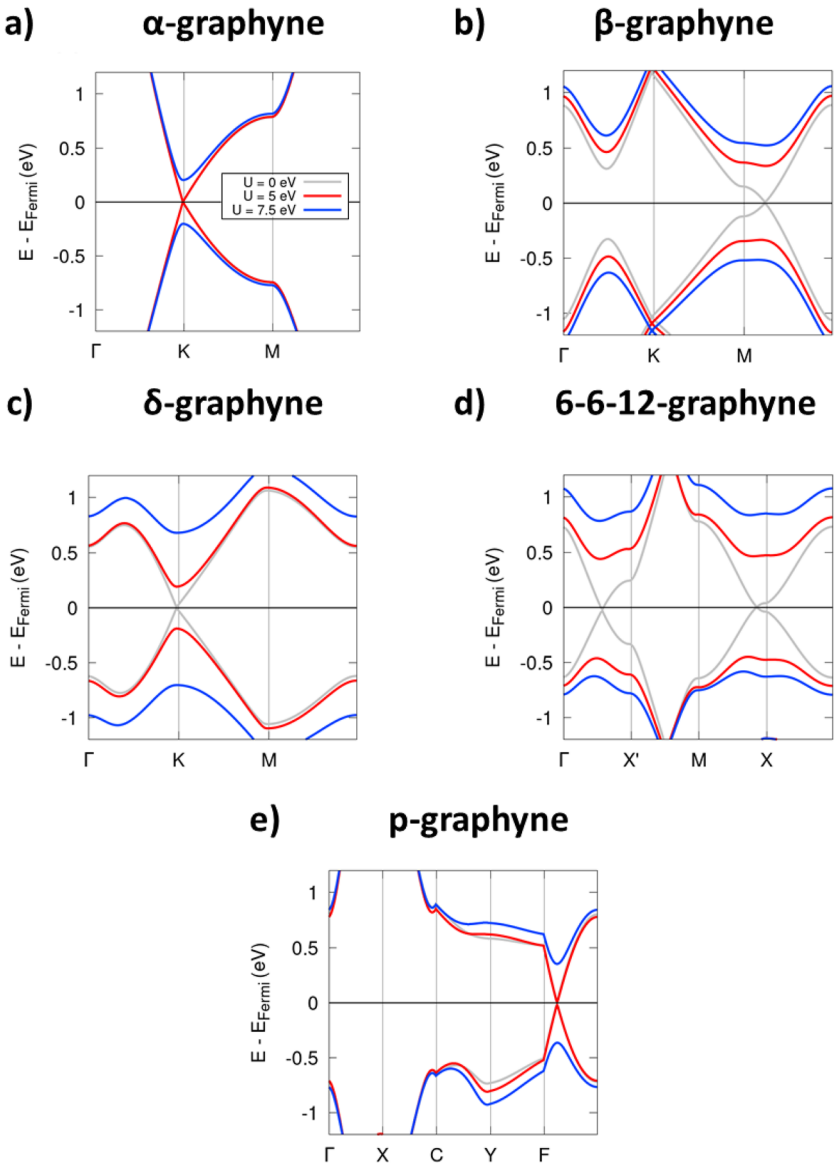

FIG. 6. Electronic band structures of (a) α-graphyne, (b) β-graphyne, (c) δ-graphyne, (d) 6-6-12 graphyne, and (e) p-graphyne. The gray bands are obtained with DFT calculations using the pure GGA (PBE) functional. The red bands are obtained using PBE + U calculations with U_{eff} = 5 eV, while the blue bands correspond to U_{eff} = 7.5 eV.

2D materials exhibiting mechanically tunable inter-sp^2 interactions could provide alternative versatile platforms for exploring correlated electronic states.[30,15]

CONCLUSIONS

In summary, we first show that by tuning the HFE percentage in a hybrid DFT approach, we can semi-quantitatively reproduce accurate results from benchmark QMC calculations for the SEM-AFI crossover in biaxially strained graphene. We further demonstrate that α-graphyne behaves in an electronically analogous manner to biaxially strained graphene with respect to the SEM-AFI crossover. In contrast, pure GGA-based calculations are unable to describe these correlated AFI solutions for physically realizable strains. Applying our tuned hybrid DFT approach to biaxially strained α-graphyne, we find that it lies at the crossover region between SEM and AFI states. Corresponding calculations on δ-graphyne and p-graphyne show a similar behavior, while β-graphyne and 6-6-12 graphyne exhibit dominant correlated gapped AFI states. We also show that the susceptibility of graphynes to exhibit correlated AFI states can also be recovered by DFT + U calculations with moderate U_{eff} values. Generally, our results suggest that graphynes are not as purely graphenic (i.e., Dirac-like) as previously proposed. However, the potential to access both SEM and gapped/spin-polarized AFI states (especially in the case of structures such as α-graphyne, δ-graphyne, and p-graphyne) makes graphynes highly attractive materials for spintronic/electronic devices and fundamental studies of correlated 2D systems.

SUPPLEMENTARY MATERIAL

See the supplementary material for comparison of QMC data for biaxially strained graphene with corresponding results from DFT calculations using the screened hybrid HSE functional with 25% and 12.5% HFE.

ACKNOWLEDGMENTS

This work was supported by the following research Grant Nos. PID2021-127957NB-I00, PID2019-109518GB-I00, TED2021-132550B-C21 (Ministerio de Ciencia e Innovación), CEX2021-001202-M ("María de Maeztu" program for Spanish Structures of Excellence), and 2017SGR13 (Generalitat de Catalunya). We also acknowledge access to supercomputer resources as provided through grants from the Red Española de Supercomputación.

AUTHOR DECLARATIONS

Conflict of Interest

The authors have no conflicts to disclose.

Author Contributions

G.L. performed all the hybrid DFT calculations for strained graphene and the graphynes. M.L.-S. performed the DFT + U calculations for the graphynes. S.T.B. wrote the manuscript. S.T.B. and I.P.R.M. coordinated the work. All authors discussed the results and methods and contributed to the final manuscript preparation.

Genis Lleopart: Conceptualization (equal); Data curation (equal); Formal analysis (equal); Funding acquisition (equal); Investigation (lead); Methodology (equal); Project administration (equal); Resources (equal); Supervision (equal); Validation (equal); Visualization (lead); Writing – original draft (lead); Writing – review & editing (supporting). **Miquel Lopez-Suarez**: Conceptualization (equal); Formal analysis (supporting); Funding acquisition (equal); Investigation (equal); Methodology (equal); Project administration (equal); Resources (equal); Supervision (equal); Validation (equal); Visualization (supporting); Writing – review & editing (supporting). **Ibério de P. R. Moreira**: Conceptualization (equal); Formal analysis (equal); Funding acquisition (equal); Investigation (supporting); Methodology (equal); Project administration (equal); Resources (equal); Supervision (equal); Validation (equal); Visualization (supporting); Writing – review & editing (supporting). **Stefan T. Bromley**: Conceptualization (equal); Data curation (equal); Formal analysis (equal); Funding acquisition (equal); Investigation (lead); Methodology (equal); Project administration (equal); Resources (equal); Supervision (equal); Validation (equal); Visualization (lead); Writing – original draft (lead); Writing – review & editing (lead).

DATA AVAILABILITY

The data that support the findings of this study are available from the corresponding authors upon reasonable request.

REFERENCES

[1] R. H. Baughman, H. Eckhardt, and M. Kertesz, J. Chem. Phys. **87**, 6687 (1987).
[2] K. Srinivasu and S. K. Ghosh, J. Phys. Chem. C **116**, 5951 (2012).
[3] Y. Li, L. Xu, H. Liu, and Y. Li, Chem. Soc. Rev. **43**, 2572 (2014).
[4] K. Khan, A. K. Tareen, M. Iqbal, Z. Shi, H. Zhang, and Z. Guo, Nano Today **39**, 101207 (2021).
[5] T. He, Y. Kong, A. R. Puente Santiago, M. A. Ahsan, H. Pan, and A. Du, Mater. Chem. Front. **5**, 6392 (2021).
[6] B. G. Kim and H. J. Choi, Phys. Rev. B **86**, 115435 (2012).
[7] D. Malko, C. Neiss, F. Vines, and A. Görling, Phys. Rev. Lett. **108**, 086804 (2012).
[8] J. Chen, J. Xi, D. Wang, and Z. Shuai, J. Phys. Chem. Lett. **4**, 1443 (2013).
[9] H.-K. Tang, E. Laksono, J. N. B. Rodrigues, P. Sengupta, F. F. Assaad, and S. Adam, Phys. Rev. Lett. **115**, 186602 (2015).
[10] S. Sorella, K. Seki, O. O. Brovko, T. Shirakawa, S. Miyakoshi, S. Yunoki, and E. Tosatti, Phys. Rev. Lett. **121**, 066402 (2018).
[11] V. Blum, R. Gehrke, F. Hanke, P. Havu, V. Havu, X. Ren, K. Reuter, and M. Scheffler, Comput. Phys. Commun. **180**, 2175 (2009).
[12] I. Y. Zhang, X. Ren, P. Rinke, V. Blum, and M. Scheffler, New J. Phys. **15**, 123033 (2013).
[13] J. P. Perdew, K. Burke, and M. Ernzerhof, Phys. Rev. Lett. **77**, 3865 (1996).
[14] S. R. Jensen, S. Saha, J. A. Flores-Livas, W. Huhn, V. Blum, S. Goedecker, and L. Frediani, J. Phys. Chem. Lett. **8**, 1449 (2017).
[15] C. Adamo and V. Barone, J. Chem. Phys. **110**, 6158 (1999).
[16] H. Xiang, C. Lee, H.-J. Koo, X. Gong, and M.-H. Whangbo, Dalton Trans. **42**, 823 (2013).
[17] S. L. Dudarev, G. A. Botton, S. Y. Savrasov, C. J. Humphreys, and A. P. Sutton, Phys. Rev. B **57**, 1505 (1998).
[18] J. M. Soler, E. Artacho, J. D. Gale, A. García, J. Junquera, P. Ordejón, and D. Sánchez-Portal, J. Phys.: Condens. Matter **14**, 2745 (2002).

[19]J. Hubbard, Proc. R. Soc. London, Ser. A **276**, 238 (1963).
[20]S. Sorella, Y. Otsuka, and S. Yunoki, Sci. Rep. **2**, 992 (2012).
[21]S.-H. Lee, H.-J. Chung, J. Heo, H. Yang, J. Shin, U.-I. Chung, and S. Seo, ACS Nano **5**, 2964 (2011).
[22]P. Rivero, I. de. P. R. Moreira, and F. Illas, Phys. Rev. B **81**, 205123 (2010).
[23]I. de. P. R. Moreira, F. Illas, and R. L. Martin, Phys. Rev. B **65**, 155102 (2002).
[24]F. Tran, P. Blaha, K. Schwarz, and P. Novák, Phys. Rev. B **74**, 155108 (2006).
[25]D. Muñoz, N. M. Harrison, and F. Illas, Phys. Rev. B **69**, 085115 (2004).
[26]V. Barone and P. Cimino, J. Chem. Theory Comput. **5**, 192 (2009).
[27]D. Reta-Mañeru, A. K. Pal, I. de. P. R. Moreira, S. N. Datta, and F. Illas, J. Chem. Theory Comput. **10**, 335 (2014).
[28]D. Cho, K. C. Ko, and J. Y. Lee, Int. J. Quantum Chem. **116**, 578 (2016).
[29]D. Reta, I. de. P. R. Moreira, and F. Illas, J. Chem. Theory Comput. **12**, 3228 (2016).
[30]I. Alcón, F. Viñes, I. de. P. R. Moreira, and S. T. Bromley, Nat. Commun. **8**, 1957 (2017).
[31]I. Alcón, R. Santiago, J. Ribas-Arino, M. Deumal, I. de. P. R. Moreira, and S. T. Bromley, Nat. Commun. **12**, 1705 (2021).
[32]R. Santiago, I. Alcón, J. Ribas-Arino, M. Deumal, I. de. P. R. Moreira, and S. T. Bromley, Adv. Funct. Mater. **31**, 2004584 (2021).
[33]J. Heyd, G. E. Scuseria, and M. Ernzerhof, J. Chem. Phys. **118**, 8207 (2003).
[34]S.-H. Lee, S. Kim, and K. Kim, Phys. Rev. B **86**, 155436 (2012).
[35]Y. Zhao and D. G. Truhlar, J. Chem. Phys. **125**, 194101 (2006).
[36]*CRC Handbook of Chemistry and Physics*, 90th ed., edited by D. R. Lide (CRC Press, 2009).
[37]K. Kaiser, L. M. Scriven, F. Schulz, P. Gawel, L. Gross, and H. L. Anderson, Science **365**, 1299 (2019).
[38]A. J. Stasyuk, O. A. Stasyuk, M. Solà, and A. A. Voityuk, Chem. Commun. **56**, 352 (2020).
[39]B. Dong, H. Guo, Z. Liu, T. Yang, P. Tao, S. Tang, R. Saito, and Z. Zhang, Carbon **131**, 223 (2018).
[40]C. Poidevin, J.-P. Malrieu, G. Trinquier, C. Lepetit, F. Allouti, M. E. Alikhani, and R. Chauvin, Chem. - Eur. J. **22**, 5295 (2016).
[41]J. L. Marshall, F. Arslan, J. A. Januszewski, M. J. Ferguson, and R. R. Tykwinski, Helvetica Chim. Acta **102**, e1900001 (2019).
[42]H. Kim, Y. Kim, J. Kim, and W. Y. Kim, Carbon **98**, 404 (2016).
[43]B. Himmetoglu, A. Floris, S. de Gironcoli, and M. Cococcioni, Int. J. Quantum Chem. **114**, 14 (2014).
[44]N. E. Kirchner-Hall, W. Zhao, Y. Xiong, I. Timrov, and I. Dabo, Appl. Sci. **11**, 2395 (2021).
[45]Y. Cao, V. Fatemi, A. Demir, S. Fang, S. L. Tomarken, J. Y. Luo, J. D. Sanchez-Yamagishi, K. Watanabe, T. Taniguchi, E. Kaxiras, R. C. Ashoori, and P. Jarillo-Herrero, Nature **556**, 80 (2018).